Radioluminescence Processes in Cerium-doped Silica Glasses

I. Zghari, H. El Hamzaoui, B. Capoen, Andy Cassez, Géraud Bouwmans, Laurent Hay, Y. Ouerdane, A. Morana, S. Girard, A. Boukenter, et al.

Radioluminescence Processes in Cerium-doped Silica Glasses

Journal:	*IEEE Transactions on Nuclear Science*
Manuscript ID	TNS-00561-2022
Manuscript Type:	RADECS 2022
Date Submitted by the Author:	29-Sep-2022
Complete List of Authors:	zghari, Ismail; Université de Lille, laboratoire PhLAM El Hamzaoui, Hicham; Université de Lille, Laboratoire PhLAM Capoen, Bruno; Université de Lille, PhLAM, UMR 8523 Cassez, Andy; Université de Lille Bouwmans, Geraud; Université de Lille, PhLAM, UMR 8523 Hay, Laurent; Université de Lille OUERDANE, Youcef; Université Saint-Etienne, UMR-CNRS 5516 Morana, Adriana; Université de Lyon, Laboratoire Hubert Curien GIRARD, Sylvain; CEA, DIF Boukenter, Aziz; Université Jean Monnet, Laboratoire H. Curien Bouazaoui, Mohamed; Université de Lille, PhLAM, UMR 8523 Benabdesselam, Mourad; Université de Nice Sophia Antipolis, Laboratoire Physique de la Matière Condensée Mady, Franck; Université de Nice Sophia Antipolis, LPMC-CNRS UMR 7336
Standard Key Words:	Radioluminescence, Cerium, silica glasses, Dosimetry, X-rays, Modeling

There May Be a Dataset Associated with This Manuscript

During the submission process, authors are asked if there is a dataset at IEEE DataPort. We provide their responses here.

Do you have DATA associated with your article?

No

IEEE DataPort DOI: CUST_DATA_DOI :No data available.

IEEE DataPort Title: CUST_DATA_TITLE :No data available.

DOI and Title of Data/Dataset not published on IEEE DataPort:

CUST_NOT_PUBLISHED_ON_DATAPORT :No data available.

Radioluminescence Processes in Cerium-doped Silica Glasses

I. Zghari, H. El Hamzaoui, B. Capoen, A. Cassez, G. Bouwmans, L. Hay, Y. Ouerdane, A. Morana, *Member, IEEE*, S. Girard, *Senior Member, IEEE,* A. Boukenter, M. Bouazaoui, M. Benabdesselam and F. Mady

***Abstract*— Rare-earth-doped silica glasses are promising materials for ionizing radiation dosimetry. In this paper, a bulk glassy silica doped with Ce ions, was prepared via the sol-gel technique and drawn at about 2000 °C into a cylindrical capillary rod. Under X-rays, this sample presents interesting radioluminescence (RL) signal properties for photon flux (dose rate) real-time monitoring. In order to elucidate RL signal dynamics associated with free carriers trapping-detrapping and recombination during and after X-ray irradiation, we studied the obtained RL signals using a kinetic model involving one or several trapping states and one recombination center. With this model and using appropriate sets of trapping parameters, extracted from the thermoluminescence data, the RL signal was numerically simulated, along with the populations of the relevant traps and centers. Several experimentally observed characteristics of the RL signals were explained using the model.**

***Index Terms*— Radioluminescence, Cerium, silica glasses, dosimetry, X-rays, Modeling.**

I. Introduction

The discovery of ionizing radiations and the development of the associated techniques paved the way to their use in different domains such as medicine (radiotherapy and diagnosis), food sterilization and fundamental physics [1-5]. However, the use of ionizing radiations requires strict measurements in terms of radiation protection in order to reduce their risks to human health and to environment. Therefore, several studies have been conducted to develop radiation detection systems capable of providing accurate and precise measurements of the radiation dose/dose rate. Among the existing passive optical dosimeters, the main used phenomena are thermoluminescence (TL), optically stimulated luminescence (OSL), and Radiation-induced attenuation (RIA), which consists in measuring the dose deposited after the end of the exposure to the rays. Radioluminescence (RL) can be exploited for the design of active dosimeters [6-8]. The RL-based dosimetry consists in measuring the spontaneous luminescence due to the prompt recombination of the radiation-induced electron-hole pairs directly during the irradiation, without the need of a stimulation heat or light to release the charges as in TL and OSL, respectively. This technique is very suitable for the field of radiotherapy, being given its real-time response to the exposure of the sensing material.

Due to its intrinsic immunity to electromagnetic interference, small size, flexibility, high sensibility, and its ability for remote interrogation [9-11], the optical fiber-based dosimetry has attracted increased attention in medical physics (radiotherapy, dosimetry and diagnosis) [12-20], but also appears very promising for beam instrumentation and dosimetry at radiation facilities or for space applications [2].

In this field, cerium-activated silica glasses are widely studied. Indeed, Ce^{3+}-doped glasses excited by UV lasers or X-rays exhibits emission signals in the blue region [6]. The emission band is assigned to the 4f-5d transition of Ce^{3+} ions with a lifetime of the ns order [7]. Moreover, this cerium doping is of great interest for dosimetry, particularly in terms of radiation hardening, because of its ability to reduce the formation of radio-induced colored centers [21-23]. For example, in [4, 6], radiation-induced luminescence properties of a Ce-doped glassy rod were studied under X-ray, and a RL response linear with dose rate was found between 10 µGy/s and 10 Gy/s. In optical fiber doped with Ce^{3+}, a linear RL intensity response has also been found in the dose rate interval 330 µGy/s to 22.6 Gy/s, as reported in [24].

The mechanisms involved in the RL process as a function of dose rate, such as electron-hole pairs creation, trapping, detrapping and recombinations can lead to write coupled differential equations, that can help to understand charge carrier kinetics in the active material. The solutions of these differential equations describe the charge carrier concentrations

Manuscript received September 29th, 2022. This work was supported in part by the Agence Nationale de la Recherche through the project FIDELIO (ANR-20-CE19-0024) and LABEX CEMPI (ANR-11-LABX-0007), as well as by the Ministry of Higher Education and Research, Hauts-de-France Regional Council and European Regional Development Fund (ERDF) through the Contrat de Projets Etat-Region (CPER Photonics for Society P4S).

I. Zghari, H. El Hamzaoui, B. Capoen, G. Bouwmans, A. Cassez, L. Hay, and M. Bouazaoui are with Univ-Lille, CNRS, UMR 8523 PhLAM-Physique des Lasers Atomes et Molécules, F-59000 Lille, France (e-mail : ismail.zghari@univ-lille.fr).

Y. Ouerdane, A. Morana, A. Boukenter, and S. Girard are with UJM, CNRS, IOGS, Laboratoire Hubert Curien, University of Lyon, UMR 5516, 18 rue Prof. B. Lauras, F-42000 Saint-Etienne, France.

F. Mady and M. Benabdesselam are with CNRS UMR 7010, Institut de Physique de Nice (INPHYNI), Université Côte d'Azur, 06108 Nice, France.

as a function of time, allowing the calculation of the RL signal. We note that this system of equations was widely used to explain TL and OSL phenomena in different materials [25-34]. However, this was limited to doped crystals for RL [35-37]. To the best of our knowledge, no RL modeling has been performed for Ce^{3+}-doped silica glasses.

Hence, this study aims to measure RL signals of Ce^{3+}-doped silica glass, at different dose rates, and to suggest a model able to qualitatively reproduce these RL signals. Based on a set of rate equations, which describe the charge traffic between the localized and delocalized bands, the numerical simulations will be performed using MATLAB programming software.

II. Materials and Methods

A. Investigated Sample

A sample of ionic cerium-doped glassy rods was synthetized using the sol-gel technique at FiberTech Lille platform of the University of Lille, as described elsewhere [38]. Then, this rod was drawn at a temperature of about 2000°C down to a submillimeter-sized cane. For RL measurements, the experimental setup was composed of 1 cm-long piece of the Ce^{3+}-doped cane spliced to 5 m long and 220 µm diameter radiation-hard multimode optical fiber supplied by iXblue.

B. RL Experimental Setup

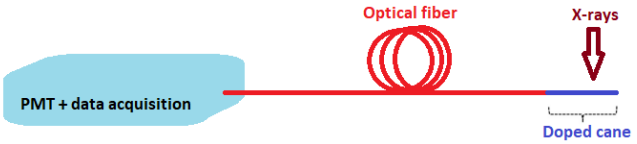

Fig. 1. Schematic illustration of the experimental setup used to characterize the RL response of the Ce^{3+}-doped cane exposed to X-ray beam.

The external X-ray beam was delivered by the LABHX facility of Laboratoire Hubert Curien, operating at 100 kV and generating photons of ~ 40 keV average energy. The X-ray dose rate was driven by the electric current of the equipment. The 1 cm-long piece of the doped cane was placed in a calibrated position of the X-irradiator. Under X-ray, the RL signal was then guided through the transport fiber toward a photomultiplier module (PMT, H9305-13 Hamamatsu). The acquisition is set with a numerical oscilloscope (Rohde & Schwarz RTM 3004). The dose rate at the various locations has been measured with an ionization chamber. All the values of dose rate and dose have been converted by considering the effective Z number ratio Z_{eff}(water)/Z_{eff}(silica). Doses are consequently given in Gy(silica) unit.

RL spectra were collected, at room temperature, by exchanging the PMT detector for a UV/VIS mini-spectrometer (Ocean Insight QE PRO) in Fig. 1. For each RL spectrum, the dark signal, due to the device, was subtracted before analysis.

III. Experimental Results

A. RL spectra

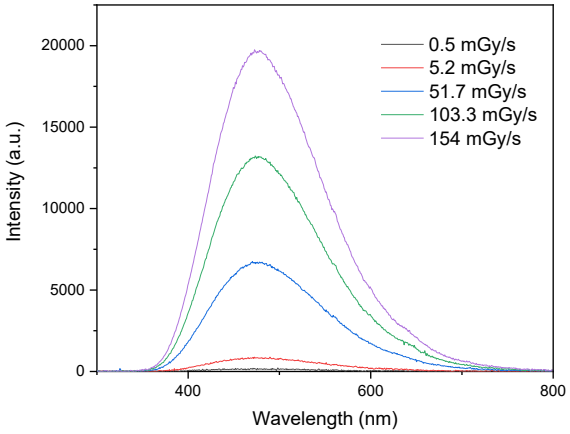

Fig. 2. RL spectra of the cerium-doped silica cane spliced to a transport fiber obtained at different X-ray dose rates.

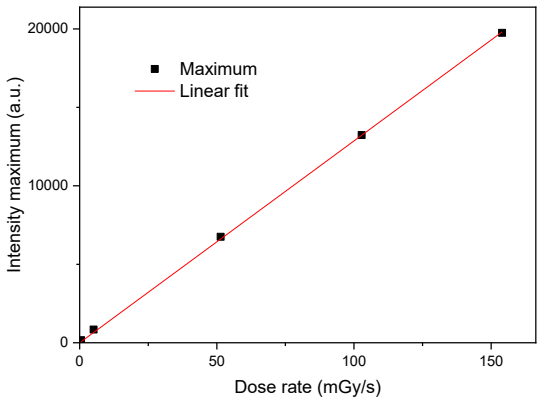

Fig.3. The dose rate dependence of the RL intensity, evaluated as the maximum of Ce^{3+} ions emission in the 0.5-154 mGy/s range.

Fig. 2. shows the RL spectrum of the Ce-doped silica cane obtained under different dose rates in the 0.5-154 mGy/s range. As reported in the literature, the spectra feature a broad emission band, peaking around 460 nm, related to the allowed 5d-4f radiative transition of Ce^{3+} ions [7]. The spectra keep the same shape and no significant modification can be observed in this range of dose rate. This result shows that Ce^{3+} ions constitute the recombination centers at the origin of the RL signal and their silica host local environment did not change with dose rate in the investigated range. Moreover, the preservation of the spectrum shape also indicates that no RIA effect alters the RL emission.

In Fig.3. we plotted the RL maximum intensity as function of dose rate. This intensity increases with the dose rate and shows a linear behavior as function of the dose rate in the 0.5-154 mGy/s range. This behavior is explained by the relation existing between the number of created electron-hole pairs and the dose rate.

B. *Integral RL signal*

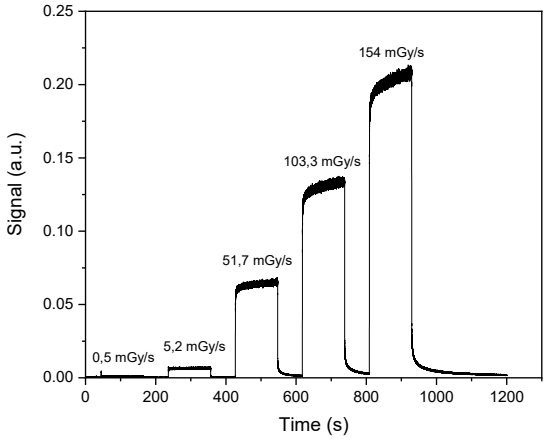

Fig. 4. RL signal response of the cerium-doped silica cane spliced to a transport fiber as a function of the X-ray dose rate.

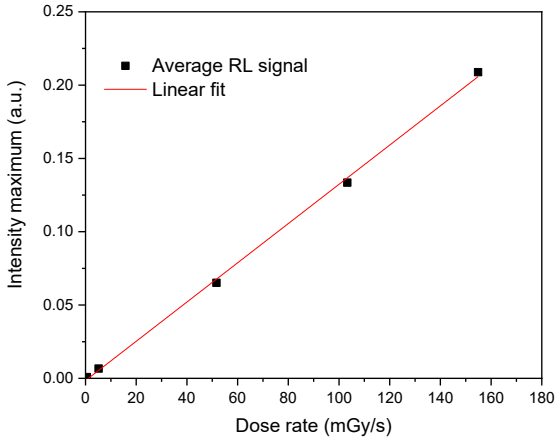

Fig.5. Dose rate dependence of the RL signal response of the cerium-doped silica cane exposed to irradiation at different X-ray dose rates. Each point represents the average RL signal, in the permanent regime (plateau).

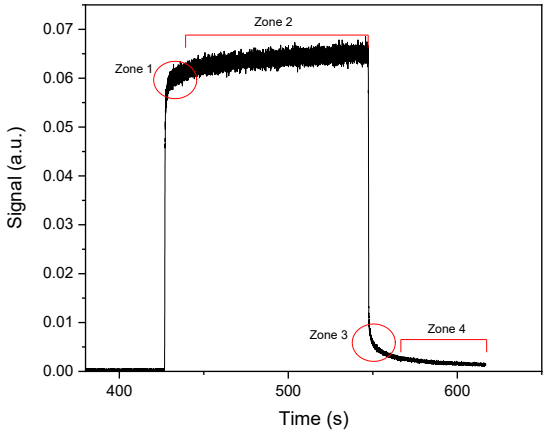

Fig.6. Example of the RL signal dynamics from the cerium-doped silica sample at a dose rate of 51.7 mGy/s, and indication of different zones that characterize the signal shape.

The RL signal evolution as a function of time for the cerium-doped sample, recorded using the PMT module at different dose rates is shown in Fig. 4. Independently of the dose rate, at the beginning of the irradiation, the experimental RL signal response is characterized by an initial abrupt jump from the background level. Then it undergoes a slower rise to finally reach a plateau. Moreover, immediately after stopping the irradiation, the signal shows a fast decrease, then exhibits an afterglow behavior (phosphorescence). It is worth noting that in our measurement conditions (40 keV X-ray), the measured RL signals are not influenced by the Cerenkov effects. Moreover, in our setup, the transport fiber was protected by a thick lead cover.

Fig. 5. shows the evolution of the average RL signal, in the permanent regime (plateau), versus the X-ray dose rate. This dependence between RL signal and dose rate shows a linear trend overall the dose rate range 0.5-154 mGy/s.

As can be seen from the example at 51.7 mGy/s (Fig. 6), two phenomena occur after the initial abrupt increase or decrease of RL signal. The first one is observed when the irradiation is turned on and the second one when it is turned off. Concerning the first one, the RL signal increases and tends toward a plateau in a few seconds. However, two characteristic zones can be distinguished, as illustrated in Fig. 6: zone 1, where the increase of RL signal slows down before reaching the plateau and zone 2 related to the plateau, which in fact consists of a faster or slower increase in the amplitude, depending on the dose rate. These two phenomena are due to shallow traps as it will be demonstrated through the modeling results in this paper. Similarly to the phenomena observed under irradiation, two characteristic zones (3) and (4) can be distinguished, corresponding to intermediate and slower decay afterglows, respectively. Shallow traps are also at the origin of the afterglow phenomenon, due to electron thermal detrapping at room temperature, after the end of irradiation.

IV. THE MODEL

To simulate our experimental results, we used a kinetic model of the trapping-recombination processes involved in the active material. Fig. 7 shows the processes described by the model, assuming that, under X rays, electron-hole pairs are generated in conduction band (CB) and valence band (VB) (process 1) respectively. Electrons can be trapped by a set of discrete trapping levels (process 2), and then thermally released (process 3) by the effect of ambient temperature, or recombine with holes on recombination center (RC) (process 4), which leads to a light emission of energy *hv (h:* Planck constant*, v:* frequency*)*. It is worthy to note that the thermal release of trapped electrons at ambient temperature must be explicitly considered, because it makes it possible to explain the dynamics of the phenomena produced during the irradiation and after the end of the irradiation.

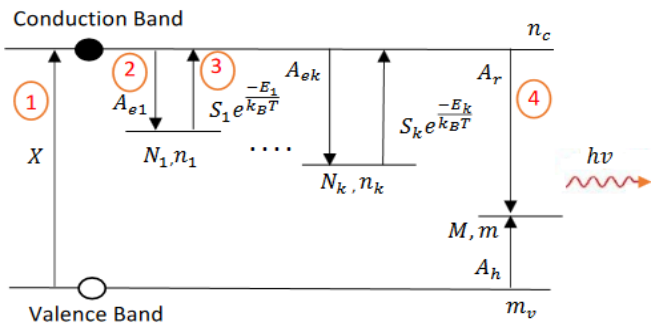

Fig. 7. Diagram depicting the energy levels and transitions involved in the mechanism of RL signal with k electrons trap states and one recombination center. The arrows 1, 2, 3, and 4 indicate the allowed transitions of electrons during RL.

N_i are the concentrations of electron traps in the level i, characterized by its energy depth E_i in the band gap. k is the number of electron trap levels. n_i are the concentrations of electrons in the traps of level i. M is the concentration of recombination centers and m is the concentration of holes in recombination center. n_c and m_v are the instantaneous concentrations of electrons and holes in the delocalized bands CB and VB, respectively. X is the rate of electron-hole pairs production, which is proportional to the excitation dose rate. A_{ei} and A_r are the transition coefficients for electrons from the conduction band to traps and recombination center, respectively. A_h is the transition coefficient for holes from the valence band to the recombination center. The parameters s_i are the corresponding frequencies factors, E_i are the activation energies of the traps, and k_B is the Boltzmann constant.

The set of coupled differential equations describing electron and hole concentrations, in the delocalized and the localized bands, governing the RL process during excitation with ionizing radiation, is as follows:

$$\frac{dn_c}{dt} = X - \sum_{i=1}^{k} n_c(N_i - n_i)A_{e_i} + \sum_{i=1}^{k} n_i s_i \, exp\left(\frac{-E_i}{k_B T}\right) - n_c A_r m \quad (1)$$

$$\frac{dm_v}{dt} = X - m_v(M - m)A_h \quad (2)$$

$$\vdots$$

$$\frac{dn_i}{dt} = n_c(N_i - n_i)A_{e_i} - n_i s_i \, exp\left(\frac{-E_i}{k_B T}\right) \quad (3)$$

$$\vdots$$

$$\frac{dm}{dt} = m_v(M - m)A_h - n_c A_r m \quad (4)$$

$$\frac{dn_c}{dt} + \sum_{i=1}^{k} \frac{dn_i}{dt} = \frac{dm_v}{dt} + \frac{dm}{dt} \quad (5)$$

Equations (1-4) govern the RL process. Equation (1) represents the variation with time of the electron concentration in the CB. The right-hand terms are as follows: the first describes the creation rate of electron–hole pairs. The second and the third represent the electron trapping and thermal detrapping rates by and from the point defect, respectively. The last one, describes the recombination rate of electron-hole pairs. Equation (2) represents the variation with time of the hole concentration in the VB. The term $m_v(M - m)A_h$ describes the holes captured by RC. Equations (3) and (4) describe the time evolution of electron and hole concentrations in the k^{th} trap and RC, respectively. Equation (5) represents electrical neutrality (the numbers of created electrons and holes are equal). This latter equation is used only to check the final result of each simulation.

The instantaneous RL intensity of the emitted light corresponds to the recombination rate of free electrons with trapped holes in the RC and it is given by the following equation:

$$I_{RL} = n_c A_r m \quad (6)$$

The values of the parameters in equations (1-4) can be determined from the experimental data or alternatively, using a fit of the model to experimental RL measurements. In our case, Ce^{3+} ions were considered as the recombination centers, as demonstrated by the RL spectra measurements and their concentration M was estimated experimentally. Concerning the nature of trapping levels, as widely reported in the literature [39-41], in the case of pure and RE-doped bulk silica, oxygen-deficient centers appear to be the most likely candidates to act as electron traps. Ce^{4+} ions may also be added as traps, due to their electron capture potential. The concentrations values of each trap state (N_i) were manually adjusted until their validity was found for all the dose rates. The activation energies E_i of the trap states were determined using TL data through initial rise method with partial cleaning method. The values used in this study are based on the results of our group reported in [4]. It is worth noting that in our case, the process of thermoluminescence is described by first-order kinetics. This means that the probability of re-trapping is negligible compared to that of recombination, which is the case for all doped silica materials [42].

The frequency factors s_i were then determined by the relation:

$$s_i = \frac{\beta E_i}{k T_{mi}^2} \exp\left(\frac{E_i}{k T_{mi}}\right) \quad (7)$$

β is the heating rate used in TL experiment, T_{mi} the temperature of the TL peak maximum corresponding to the trap of energy E_i. These parameters were deduced from the thermoluminescence glow curve [4].

The pair creation rate X is associated with the dose rate used during the RL measurement. Hence, the value of X was estimated from the dose rate, the SiO_2 glass density (d = 2.3

g/cm^3), the electron-hole pair creation energy E_p = 17 eV [43-44].

For the given value of E_p, the initial density of electron-hole pairs per dose unit is determined by:

$$\eta = \frac{d}{E_p} = 0.135\ \mathrm{g.eV^{-1}.cm^{-1}} = 8.44 \times 10^{12}\mathrm{rad^{-1}.cm^{-1}}$$
$$= 8.44 \times 10^{14}\mathrm{Gy^{-1}cm^{-3}}$$

where 1 rad = 100 erg/g = 6,24.1013 eV/g

Thus, any dose rate in Gy.s^{-1} will be multiplied by this value to determine the value of X in cm^{-3}.s^{-1}. The transition coefficients (A_{ei}, A_r, and A_h) have been found by optimizing the four (1-4) differential equations with a least-square method using dedicated programming software. It can be stressed here that we are not interested in the exact values of these coefficients but rather in their ratio. Indeed, the competition between trapping and recombination processes is well reflected by the ratio between A_{ei} and A_r, for example [37].

V. Results and Discussion

A. RL signal simulation

In order to simulate the RL signal as a function of time at different dose rates, the set of equations (1-4) was solved numerically using MATLAB software. The values of the different parameters used in this simulation are summarized in Table I. It should be noted that for all dose rates, these values are unchanged.

TABLE I
PARAMETER VALUES USED IN THE SIMULATIONS.

Symbol	Parameter	Value
T	Temperature	295 K
X	Generation rate of electron-hole pairs	5.2 mGy(SiO_2)/s → 4.3×10^{12} cm^{-3}.s^{-1} 51.7 mGy(SiO_2)/s→ 4.3×10^{13} cm^{-3}.s^{-1}
E_1, E_2	Activation energies	0.85 eV and 0.94 eV
M	Concentration of recombination centers	2×10^{18} cm^{-3}
k_B	Boltzmann constant	8.617330×10^{-5} eV.K^{-1}
t_D	Irradiation time	120 s
t_f	Afterglow time	60 s
s_1, s_2	Frequency factors	~10^{14} s^{-1}
N_1, N_2	Concentrations of electrons traps	3×10^{17} and 9×10^{16} cm^{-3}

The simulation consists of two stages: irradiation time (t_D) and phosphorescence time (t_f), when the irradiation is stopped. For the first stage, the differential equations (1- 4) are solved for an irradiation time t_D, with initial conditions:

$n_c(0) \neq 0$, $n_i(0) \neq 0$, $n_v(0) \neq 0$, and $m(0) \neq 0$

because the sample has already been irradiated during the verification tests, and the RL signal is simulated by using equation (6).

For the second stage, the phosphorescence period has been simulated by setting $X=0$ and solving the same equations for a time t_f, the initial values of population concentrations corresponding to the final values of the first stage.

It should be noted that both experimental and simulated signals have been normalized to be compared. Obviously, the absolute intensity depends on a lot of experimental parameters. Thus, it can be repeated only if the experimental conditions are kept the same. The model allows to calculate the signal intensity up to a factor. Once the fitted parameters are fixed in the model, simulations are able to reproduce the experimental RL signal at every dose rate in the linearity domain.

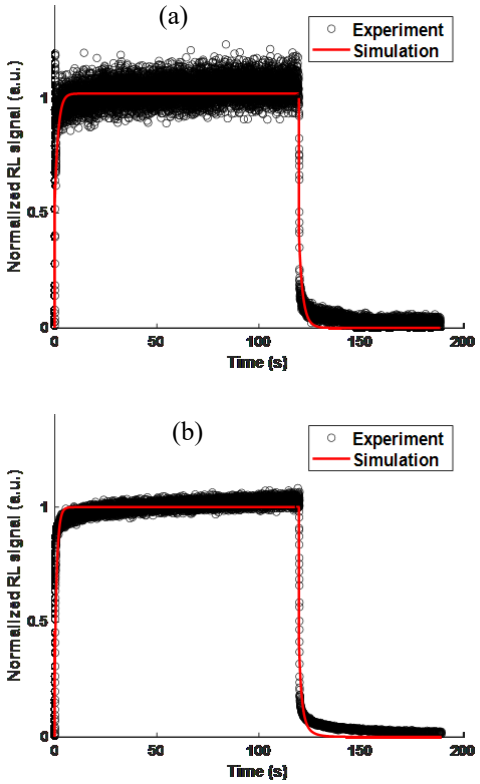

Fig. 8. Measured and simulated RL signals under X-rays with one trap at 0.85 eV under CB and one recombination center for a dose rate of 5.2 mGy/s (a) and for a dose rate of 51.7 mGy/s (b). The small peak at the beginning of the irradiation, in the curve (a), is due to the machine.

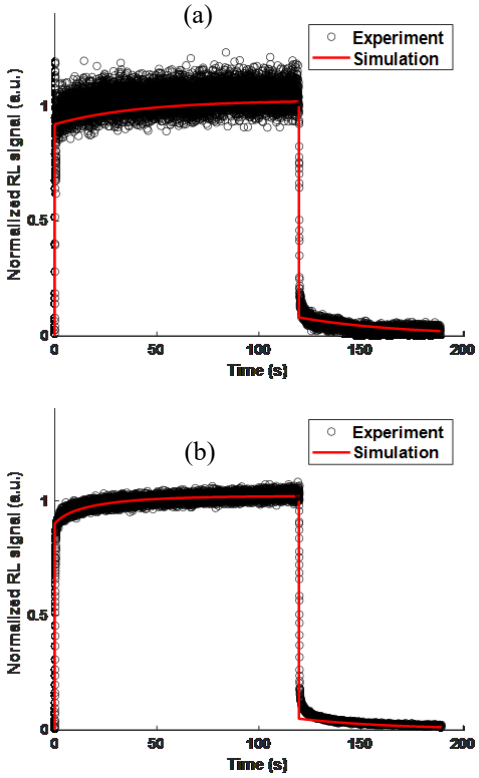

Fig. 9. Measured and simulated RL signals under X-rays with one trap at 0.94 eV under CB and one recombination center for a dose rate of 5.2 mGy/s (a) and for a dose rate of 51.7 mGy/s (b). The small peak at the beginning of the irradiation, in the curve (a), is due to the machine.

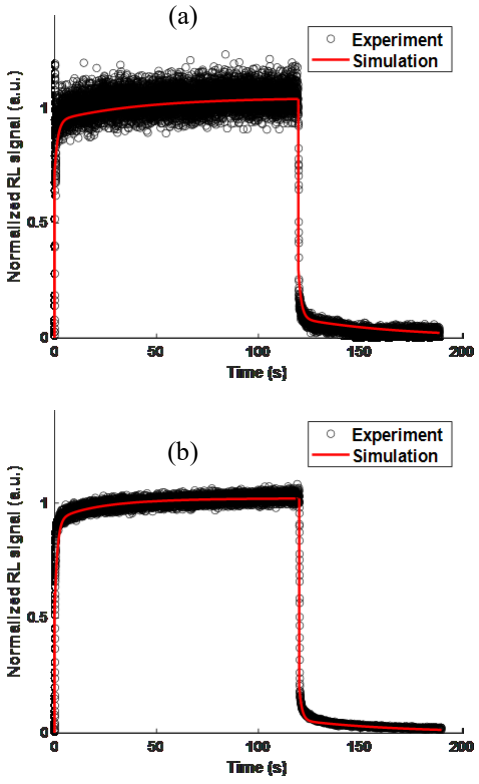

Fig. 10. Measured and simulated RL signals under X-rays with two traps (at 0.85 and 0.94 eV under CB) and one recombination center for a dose rate of 5.2 mGy/s (a) and for a dose rate of 51.7 mGy/s (b). The small peak at the beginning of the irradiation, in the curve (a), is due to the machine.

Fig. 8, Fig.9, and Fig. 10 show the RL signal evolution versus time obtained at 5.2 mGy/s and 51.7 mGy/s with one trap 0.85 eV or 0.94 eV under BC and two traps (0.85 and 0.94 eV), respectively.

The red curves in Fig. 8, Fig. 9, and Fig. 10 illustrate the simulated RL signal using one trap (at 0.85 or 0.94 eV) and two traps (at 0.85 and 0.94 eV), respectively. At first glance, independently of the dose rate or the number of traps, the numerical simulations show an overall behavior similar to the experimental data. However, under close scrutiny, the model based on one electron trap at 0.85 eV, with two dose rates (Fig.8 (a) and (b)), led to simulation curves which reproduce the experimental data (shape). In particular, contrary to the experimental curve, the simulation shows a constant plateau over time (zone 2), during irradiation, and the simulation curve quickly reaches zero (zone 4), after irradiation.

On the other hand, in Fig. 9, the model based on one electron trap at 0.94 eV led to simulation curves with a sharp transition point between the initial abrupt rise (zone 1) (or decrease) and slow rise (zone 2) (or decrease) of the RL signal.

Besides, the combination of these two electron traps (at 0.85 and 0.94 eV)) makes it possible to perfectly reproduce the experimental data in the different zones (Fig. 10). This highlights the importance of considering at least two electron traps in the mechanism of RL process. It is worth to note that the shallower trap (at 0.85 eV) could not be inferred *via* thermoluminescence (TL) measurements performed at room temperature. To characterize such shallow traps, TL measurements should be carried out under cryogenic temperature conditions. However, in our case, the TL peak corresponding to the introduced shallow trap was determined using the simplest model of TL based on a first-order kinetics process [27, 28].

In reality, there are other electron traps, either deeper than 0.94 eV or much shallower than 0.85 eV. The choice to ignore them is firstly due to the fact that they have no significant role on the signal shape under these measurement conditions. Secondly, by using only two trap levels, the number of equations can be reduced in order to minimize the risk of divergence during the simulation.

Table II summarizes the calculated ratios between the recombination and the trapping coefficients deduced from the simulation using one or two traps. These ratios are remarkably identical for both dose rates, indicating that the probability of re-trapping is negligible compared to that of recombination. We note that these values verify the kinetics of first order.

TABLE II
VALUE OF RATIO BETWEEN RECOMBINATION AND TRAPPING COEFFICIENTS OBTAINED FROM THE SIMULATION USING ONE OR TWO TRAPS

Dose rate	*5.2 mGy/s*	*52 mGy/s*
1 trap (0.85 eV)	$\frac{A_{e1}}{A_r} = 1.0223 \times 10^{-4}$	$\frac{A_{e1}}{A_r} = 1.0222 \times 10^{-4}$
1 trap (0.94 eV)	$\frac{A_{e1}}{A_r} = 1.0223 \times 10^{-4}$	$\frac{A_{e1}}{A_r} = 1.0223 \times 10^{-4}$
2 traps (0.85-0.94 eV)	$\frac{A_{e1}}{A_r} = \frac{A_{e2}}{A_r} = 1.0223 \times 10^{-4}$	$\frac{A_{e1}}{A_r} = \frac{A_{e2}}{A_r} = 1.0223 \times 10^{-4}$

B. *Simulation of trapped carrier concentration*

The two electron traps model is also able to provide the time evolution of the carrier's populations in the different energy levels.

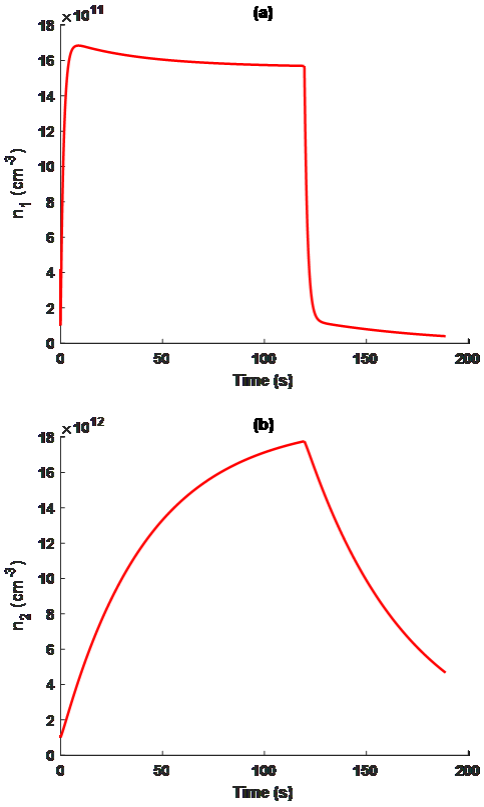

Fig. 11. Simulation of trapped carrier concentration, with the same set of parameters in the text, for a dose rate of 5.2 mGy/s for the 0.85 eV electron trap (a) and for the 0.94 eV electron trap (b).

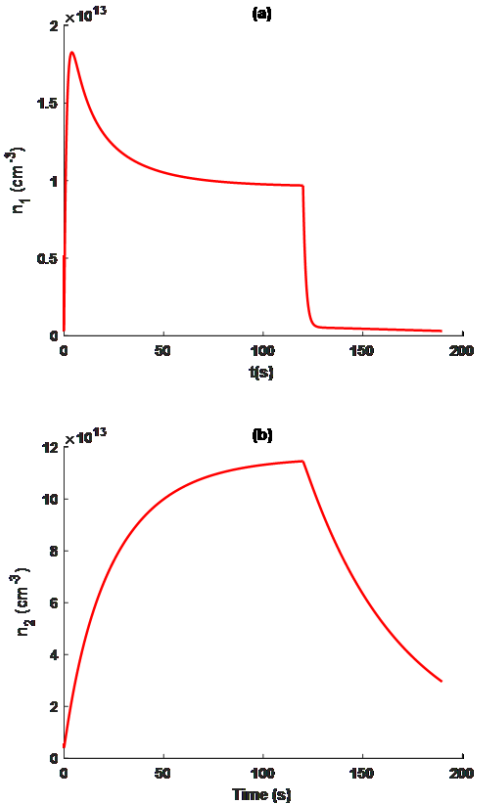

Fig. 12. Simulation of trapped carrier concentration, with the same set of parameters in the text, for a dose rate of 51.7 mGy/s for the 0.85 eV electron trap (a) and for the 0.94 eV electron trap (b).

Figures 11 and 12 show the evolutions of the 0.85 and 0.94 eV electron traps populations as a function of time, during and after stopping the X-rays irradiation, for dose rates of 5.2 and 51.7 mGy/s, respectively. We notice, as a first remark, that the overall shapes of the filling curves of each trap remain unchanged as a function of the dose rate. Only their amplitudes increase with the dose rate, since the number of the created electron-hole pairs increases. This shows that the trap filling dynamics and mechanism remain independent of the dose rate.

At the beginning of the irradiation, the concentration of trapped electrons increases. Then, after a certain time, it becomes constant (plateau) and finally decreases when the irradiation was stopped. However, these same dynamics and mechanism, governing the process of the electron trapping, do not occur within the same time scale for both the studied traps. Besides, it can be mentioned that the population curves do not start from zero, since the sample was already irradiated during the first implementation of the measurements.

Concerning the 0.85 eV trap, the detrapping of electrons begins a few seconds after irradiation, as illustrated by the curve (a) in Figs. 11 and 12 for both dose rates. Then around 40 seconds, the electron population reaches its equilibrium state between trapping and detrapping, which means that the number of trapped electrons is equal to the number of thermally detrapped electrons at ambient temperature. In addition, the concentration of trapped electrons after stopping the irradiation decreases very quickly, so that the total phosphorescence of this trap occurs only a few seconds after stopping the irradiation.

Hence, the detrapping processes involved in this trap at 0.85 eV, during and after the irradiation, are at the origin of the RL signal shape in the zone 1 and 3, respectively.

Contrary to the electron trap at 0.85 eV, the filling curve of the level at 0.94 eV as a function of time does not reach its equilibrium state, even after 120 s of irradiation and regardless of the dose rate. Furthermore, when the irradiation is stopped, the concentration of trap carriers slowly decreases. Thus, during and after irradiation, this trap at 0.94 eV is mainly involved in the zones 2 and 4 of the RL signal, respectively. The difference in detrapping times and the time required to reach the equilibrium state are related to the lifetime τ_i of the electrons in each trap, which is described by eq. (9) [27]. In this equation, the parameters are the same as in eq. (7). Hence, the deeper the trap, the longer the lifetime of the electrons in this trap.

$$\tau_i = s_i^{-1} \exp\left(\frac{E_i}{kT}\right) \quad (9)$$

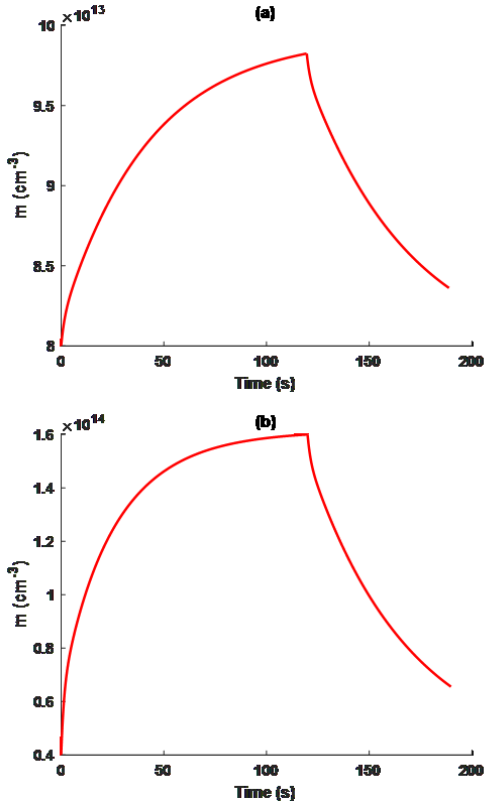

Fig. 13. Simulation of hole concentration in recombination center, for a dose rate of 5.2 mGy/s (a) and 51.7 mGy/s (b).

Figure 13 shows the evolution of the hole concentration in the recombination center during and after stopping the irradiation for the dose rates of 5.2 and 51.7 mGy/s. From the physical point of view, this concentration is equal to the total hole concentrations created minus the hole concentration recombined with the electrons. By respecting the principle of electrical neutrality, this concentration must be equal to the number of non-recombined electrons (the trapped electrons).

Independently of the dose rate, it is very clearly seen that the shape of the curve remains the same, only the concentration values increase with the dose rate. For 120 s (during irradiation), the hole concentration increases with strong damping followed by an asymptotic behavior towards a state of equilibrium. Based on our view above, this increase reflects well the increase in trapped electrons (Fig. 12).

After stopping the irradiation, two different decay rates can be visually distinguished. The first is a fast decay that occurs just after the irradiation stops and it is also due to the fast detrapping of electrons in the trap at 0.85 eV. The second one is a slow decay which reflects the slow detrapping behavior of traps at 0.94 eV.

The curves in figure 13 show the dynamics of the holes at the level of the recombination center. It should be noted here that the shapes of these curves remain valid only in the case of two traps.

VI. Conclusion

In this contribution, ionic cerium-doped glassy rods were synthetized using the sol-gel technique. After drawing, the obtained sample showed a RL broad band centered around 460 nm, attributed to the allowed 5d-4f radiative transition of Ce^{3+} ions, under X-rays in the dose rate range 0.5-154 mGy/s. Moreover, the spectral shape of the RL band remains unchanged and the intensity of the RL signal exhibits a linear behavior as a function of dose rate in this range. Besides, the average RL signal recorded with PMT module in the permanent regime (plateau), also shows a linear response versus the X-ray dose rate in the studied range.

The RL signal kinetics was numerically simulated using a kinetic model of the trapping-recombination processes involved in the active material. This allowed us to explain the RL dynamics of trapping-detrapping and recombination during and after X-ray irradiation.

The simulation shows the dynamics of the unstable traps and their assignment to the RL signal shape. We distinguished the effect of two types of unstable traps. The first one is situated at 0.85 eV under the conduction band and has a fast lifespan, so that its population quickly reaches its equilibrium state. The second one, at 0.94 eV in the gap and with a slower lifespan, has a filling curve which takes more time to reach its equilibrium state. This has been confirmed by the simulation of the concentration of trapped carriers. Indeed, the population of the unstable 0.85 eV trap reaches its equilibrium states much faster than the 0.94 eV one, where the number of electrons does not reach its equilibrium states within an irradiation time of 120 s. The population dynamics of these two types of traps explains well the fast rise (or decrease) and the slow rise (decrease) of the RL signal. Moreover, we simulated the evolution of the concentration of holes in the recombination center during and after the irradiation stop. We also showed that the dynamics of these holes are related to that of the carrier concentration in the electron traps.

Finally, it is pointed out that the results presented in this paper and their associated discussion are valid for a range of dose rates up to 1 Gy/s.

REFERENCES

[1] N. Chiodini, A. Vedda, and I. Veronese, "Rare Earth Doped Silica Optical Fibre Sensors for Dosimetry in Medical and Technical Applications," *Adv. Opt.*, vol. 2014, pp. 974584-1– 974584-9, Oct. 2014.

[2] S. Girard, A. Morana, A. Ladaci, T. Robin, L. Mescia, J.-J. Bonnefois, M. Boutillier, J. Mekki, A. Paveau, B. Cadier, E. Marin, Y. Ouerdane, and A. Boukenter, "Recent advances in radiation-hardened fiber-based technologies for space applications," *J. Opt.,* Vol. 20, no. 9, 093001, Aug. 2018.

[3] C. P. Feliciano, "High-dose irradiated food: Current progress, applications, and prospects," *Rad. Phys. Chem*. Vol. 144, pp. 34-36, Mar. 2018.

[4] M. Benabdesselam, J. Bahout, W.Blanc, H. El Hamzaoui, A. Cassez, K. Delplace-Baudelle, R. Habert, G. Bouwmans, M. Bouazaoui, and B. Capoen., "TL Properties of RE-Doped and Co-Doped Sol-Gel Silica Rods. Application to Passive (OSL) and Real-Time (RL) Dosimetry," *IEEE Sens. J.*, vol. 21, no. 24, pp. 27465-27472, 15 Dec.15, 2021

[5] I. Obodovskiy "Radiation Fundamentals, Applications, Risks, and Safety," *Elsevier*, 2019, pp 1-694

[6] N. Al Helou, H.El Hamzaoui, B. Capoen, G. Bouwmans, A. Cassez, Y. Ouerdane, A. Boukenter, S. Girard, G. Chadeyron, R. Mahiou, and M. Bouazaoui., "Radioluminescence and Optically Stimulated Luminescence Responses of a Cerium-Doped Sol-Gel Silica Glass Under X-Ray Beam Irradiation," *IEEE Trans. Nucl. Sci.*, vol. 65, no. 8, pp. 1591-1597, Aug. 2018.

[7] J. Bahout, Y. Ouerdane, H. El Hamzaoui, G. Bouwmans, M. Bouazaoui, A. Cassez, K. Baudelle, R. Habert, A. Morana, A. Boukenter, S. Girard, B. and Capoen, B. "Cu/Ce-co-Doped Silica Glass as Radioluminescent Material for Ionizing Radiation Dosimetry," *Materials*, vol. 13, no. 11, pp. 2611-1–2611-11, Jun. 2020.

[8] A.K.M. Mizanur Rahman, H.T. Zubair, Mahfuza Begum, H.A. Abdul-Rashid, Z. Yusoff, N.M. Ung, K.A. Mat-Sharif, W.S. Wan Abdullah, Ghafour Amouzad Mahdiraji, Y.M. Amin, M.J. Maah, and D.A. Bradley, "Germanium-doped optical fiber for real-time radiation dosimetry," *Radiat. Phys. Chem.*, vol. 116, pp. 170–175, Nov. 2015.

[9] B. L. Justus, P. Falkenstein, A. L. Huston, M. C. Plazas, H. Ning, and R. W. Miller, "Gated fiber-optic-coupled detector for in vivo real-time radiation dosimetry," *Appl. Opt.*, vol. 43, no. 8, pp. 1663–1668, Mar. 2004.

[10] A. Berra, V. Conti, D. Lietti, L. Milan, C. Novati, A. Ostinelli, M. Prest, C. Romanó and E. Vallazza., "A SiPM based real time dosimeter for radiotherapic beams," *Nucl. Instrum. Methods Phys. Res. A, Accel. Spectrom. Detect. Assoc. Equip.*, vol. 773, pp. 72–80, Feb. 2015.

[11] D.A Bradley, R.P Hugtenburg, A. Nisbet, A.T. Abdul Rahman, F. Issa, N. Mohd Noor, and A. Alalawi. "Review of Doped Silica Glass Optical Fibre: Their TL Properties and Potential Applications in Radiation Therapy Dosimetry," *Appl. Radiat. Isot.* vol. 71, pp. 2-11, Dec. 2012.

[12] P. Carrasco, N. Jornet, O. Jordi, M. Lizondo, A. Latorre-Musoll, T. Eudaldo, A. Ruiz, and M. Ribas, "Characterization of the Exradin W1 scintillator for use in radiotherapy," *Med. Phys.* vol. 42, no. 1, pp. 297-304, Nov. 2016.

[13] S. Girard, B. Capoen, H. El Hamzaoui, M. Bouazaoui, G. Bouwmans, A. Morana, D. Di Francesca, A. Boukenter, O. Duhamel, P. Paillet, M. Raine, M. Gaillardin, M. Trinczek, C. Hoehr, E. Blackmore, and Y. Ouerdane, "Potential of Copper- and Cerium-Doped Optical Fiber Materials for Proton Beam Monitoring," *IEEE Trans. Nucl. Sci.*, vol. 64, no. 1, pp. 567-573, Jan. 2017.

[14] C. Hoehr, C. Lindsay, J. Beaudry, C. Penner, V. Strgar, R. Lee, and C. Duzenli. "Characterization of the exradin W1 plastic scintillation detector for small field applications in proton therapy," *Phys. Med. Biol*., vol. 63, no. 9, pp. 095016, May 2018.

[15] S. O'Keeffe, D. McCarthy, P. Woulfe, MWD. Grattan, AR. Hounsell, D. Sporea, L. Mihai, I. Vata, G. Leen, and E. Lewis., "A review of recent advances in optical fibre sensors for in vivo dosimetry during radiotherapy," *Br. J. Radiol*. vol. 88, pp. 20140702, 1050 Apr. 2015.

[16] C. Penner, C. Hoehr, S.Okeeffe, P. Woulfe and C. Duzenli, "Characterization of a Terbium Activated Gadolinium Oxysulfide Plastic Optical Fibre Sensor in Photons and Protons, " *IEEE Sens. J*., vol. 18, pp. 1513-1519, Feb. 2018.

[17] E. Mones, I. Veronese, F. Moretti, M. Fasoli, G. Loi, E. Negri, M. G. Brambilla, N. Chiodini, G. Brambilla, and A. Vedda. "Feasibility study for the use of Ce^{3+}-doped optical fibres in radiotherapy," *Nucl. Instrum. Methods Phys. Res. A, Accel. Spectrom. Detect. Assoc. Equip.* vol. 562, no. 1, pp. 449-455, Jun. 2006.

[18] I. Veronese, N. Chiodini, S. Cialdi, E. d'Ippolito, M. Fasoli, S. Gallo, S. La Torre, E. Mones, A. Vedda, and G. Loi. "Real-time dosimetry with Yb-doped silica optical fibres," *Phys. Med. Biol*., vol. 62, no. 10, pp. 4218, Apr. 2017.

[19] T. Yanagida, "Study of rare-earth-doped scintillators," *Opt. Mater.*, vol. 35, no. 11, pp. 1987–1992, Sep. 2013.

[20] L. Torrisi, "Plastic scintillator investigations for relative dosimetry in proton-therapy," *Nucl. Instrum. Methods Phys. Res. B*vol. 170, no. 3-4, pp. 523-530, Oct. 2000.

[21] J. S. Stroud, "Color-Center Kinetics in Cerium-Containing Glass," *J. Chem. Phys.,* vol. 43, pp. 2442–2450, Oct. 1965.

[22] J. S. Stroud, "Color Centers in a Cerium-Containing Silicate Glass," *J. Chem. Phys.*, vol. 37, pp. 836-841, Aug. 1962.

[23] X. Fu, and L. Song, J. Li, "Radiation induced color centers in cerium-doped and cerium-free multicomponent silicate glasses," *Journal of Rare Earths*, vol. 32, pp. 1037-1042, 2014

[24] M. Cieslikiewicz-Bouet, H. El Hamzaoui, Y. Ouerdane, R. Mahiou, G. Chadeyron, L. Bigot, K. Delplace-Baudelle, R. Habert, S. Plus, A. Cassez, G. Bouwmans, M. Bouazaoui, A. Morana, A. Boukenter, S. Girard, B. Capoen, "Investigation of the incorporation of cerium ions in MCVD-silica glass preforms for remote optical fiber radiation dosimetry," *Sensors*, vol. 21, no. 10, Jan. 2021.

[25] C. Furetta, J. Roman, T. Rivera, J. C. Azorín, C. Azorín, and H.R. Vega-Carrillo, "Modeling the thermoluminescent response of $CaSO_4$:Dy by the MCNPX method," *Appl. Radiat. Isot.* vol. 68, no. 4-5, pp. 967-969, Apr. May 2010.

[26] K. Ahmed, and K. Dahane, "Modeling of the thermoluminescence mechanisms in ZrO_2," *Appl. Radiat. Isot.*, vol. 82, pp. 49-54, Dec. 2013.

[27] R. Chen, and V. Pagonis, "The role of simulations in the study of thermoluminescence (TL)," *Radiat. Meas.*, vol. 71, pp. 8-14, Dec. 2014.

[28] R. Chen, V. Pagonis, and J.L. Lawless, "Time and dose-rate dependence of TL and OSL due to competition between excitation and fading," *Radiat. Meas.*, vol. 82, pp. 115-121, Nov. 2015.

[29] A. Bouremani, D. Kadri, A. Kadari, and V. Dubey, "Modeling of thermoluminescence in $SrY_2O_4:Eu^{3+}$ and their concentration quenching effect," *Optik*, vol. 232, pp. 166607, Apr. 2021.

[30] N. Kucuk, I. Kucuk, "Computational modeling of thermoluminescence glow curves of zinc borate crystals," *J. Inequal. Appl.*, vol. 136, Mar. 2013.

[31] P. Olko, P. Bilski, M. Budzanowski, M. P. Waligórski, A. Fasso, and N. E. Ipe, "Modelling of the Thermoluminescence Response of LiF:Mg,Cu,P (MCP-N) Detectors after Doses of Low-Energy Photons," *Radiat. Prot. Dosim.*, vol. 84, no. 1-4, pp. 103-107, Aug. 1999.

[32] J. Marcazzó, M. Santiago, N. Khaidukov, and E. Caselli, "Modelling the optical bleaching of the thermoluminescence of $K_2YF_5:Pr^{3+}$,". *Radiat. Meas.*, vol. 47, no. 10, pp. 951-956, Oct. 2012.

[33] A. Kadari, N. M. Khaidukov, R. Mostefa, E. C. Silva, and L. Faria, "Trapping parameters determination and modeling of the thermoluminescence process in $K_2GdF_5:Dy^{3+}$," *Optik*, vol. 127, no. 8, Apr. 2016.

[34] A.J.J. Bos, "Thermoluminescence as a Research Tool to Investigate Luminescence Mechanisms," *Materials*, vol. 10, no. 12, pp. 1357, Nov. 2017.

[35] V. Pagonis, J. Lawless, R. Chen, and C. E. Andersen, "Radioluminescence in Al_2O_3: C - analytical and numerical simulation results," *J. Phys. D: Appl. Phys.*, vol. 42, no. 17, pp. 175107, Aug. 2009.

[36] J. J. Schuyt, J. Donaldson, G. V. M. Williams, and S. V. Chong, "Modelling the radioluminescence of Sm^{2+} and Sm^{3+} in the dosimeter material $NaMgF_3$: Sm," *J. Phys.: Condens. Matter.*, vol. 32, pp. 025703, Oct. 2019.

[37] F. Moretti, G. Patton, A. Belsky, M. Fasoli, A. Vedda, *et al.*, "Radioluminescence Sensitization in Scintillators and Phosphors: Trap Engineering and Modeling," *J. Phys. Chem. C*, vol. 118, no. 18, pp. 9670-9676, Apr. 2014.

[38] H. El Hamzaoui, B. Capoen, N. Al Helou, G. Bouwmans, Y. Ouerdane, A. Boukenter, S. Girard, C. Marcandella, O. Duhamel, G. Chadeyron, R. Mahiou, and M. Bouazaoui, "Cerium-activated sol-gel silica glasses for

radiation dosimetry in harsh environment," *Mater. Res. Express*, vol. 3, no. 4, pp. 046201-1–046201-7, Apr. 2016.
[39] A. Losavio, B. Crivelli, F. Cazzaniga, M. Martini, G. Spinolo, and A. Vedda, "Oxide damage by ion implantation in silicon," *App. Phys. Lett*, vol. 74, no. 17, 1999.
[40] A. Vedda, N. Chiodini, D. Di Martino, M. Fasoli, L. Griguta, F. Moretti, and E. Rosetta, "Thermally stimulated luminescence of Ce and Tb doped SiO_2 sol–gel glasses," *J. Non-Cryst. Solids*, Vol. 351, no. 49–51, pp. 3699-3703. Nov. 2005.
[41] M. Martini, F. Meinardi, E. Rosetta, G. Spinolo, A. Vedda, J.L. Leray, P. Paillet, J.L Autran, and R.A.B. Devine, "Radiation induced trap levels in SIMOX oxides: low temperature thermally stimulated luminescence," in *IEEE Trans. Nucl. Sci*, vol. 45, no. 3, pp. 1396-1401, June 1998.
[42] F. Mady, A. Gutilla, M. Benabdesselam, G. Wilfried, S. Girard, Y. Ouerdane, A. Boukenter, H. Desjonquères, C. M. Louvet, "Optical fibers under irradiation: quantitative assessment of the energy distribution of radiation-induced trapped states," *Proc. SPIE*, vol. 11357, Apr. 2020.
[43] N. Al Helou, "Etude de verres pour la dosimétrie fibrée de rayonnements ionisants," PhD. Université de Lille, France, 2018. p. 173.
[44] G.A. Ausman Jr., and F.B. McLean, "Electron-hole pair creation energy in SiO_2", *Appl. Phys. Lett.*, Vol. 26, no. 4, pp. 173-175, Feb. 1975.